JMEPEG (1993) 2:745-758

Effect of Long-Term 1093 K Exposure to Air or Vacuum on the Structure of Several Wrought Superalloys

J.D. Whittenberger

Long-term 1093 K heat treatments of three commercial superalloy sheet materials were undertaken in air and vacuum. With either exposure, significant precipitation of second phases occurred in the Co-base Haynes® Alloy 188 (HA 188) and the Ni-base Haynes® Alloy 230 (HA 230); however, much less precipitation was found in the exposed Ni-base alloy Inconel® 617 (IN 617). Although some grain growth occurred in HA 188, no changes in the grain size of either HA 230 or IN 617 were observed after 22,500 h at temperature. Oxidation during air heat treatments led to weight gain due to the formation of chromia + spinel scales and surface-connected grain boundary pits/oxides in all three superalloys. Both the weight gain and depth of intergranular attack were dependent on the square root of time, which is indicative of diffusion-controlled phenomena. Because many alloy samples had neighbors in close proximity, most vacuum heat treated specimens did not suffer significant loss of volatile elements. However, some exposed samples were subjected to unrestricted vacuum heat treatments, allowing estimates of volatilization to be made. Based on the data for HA 188, the weight loss during 1093 K vacuum exposure was diffusion controlled once the inhibiting effects of surface films on the as-received alloys were broken down.

Keywords

Heat treatment, oxidation, superalloys, vacuum exposure

1. Introduction

A SOLAR dynamic power system has been proposed[1] to convert heat to electricity for Space Station Freedom. For this mechanism to continue to operate while in the earth's ellipse, a means to store energy is required. The method of choice[2] uses the solid to liquid phase transformation for the eutectic salt of nominal composition (at.%) LiF-20CaF_2, which melts at 1043 K. This fluoride mixture is advantageous because (1) its heat of fusion translates into high weight and volume energy densities; (2) the melting temperature is ideal for supplying heat to a low-temperature Brayton Cycle engine; and (3) it was believed that the molten salt could be successfully encapsulated with existing superalloys.[3] Although molten LiF-20CaF_2 is probably the most egregious environmental concern for thermal energy storage containment alloys, they will also undergo long-term, elevated temperature exposures in the vacuum of space. This too can affect the performance of most superalloys, because volatile elements, such as Cr and Mn, will evaporate from vacuum-exposed surfaces, and the subsequent changes in alloy chemistry can lead to changes in microstructure and mechanical properties.[4]

A program has been initiated at the Lewis Research Center to determine the effects of very long 1093 K exposures to the LiF-CaF_2 eutectic and vacuum on the structure and mechanical properties of superalloys. This effort has been conducted to provide reassurance that existing superalloys are capable of withstanding these potentially deleterious environments. Although the majority of work has concentrated[5,6] on the Co-base materials Haynes® Alloy™ 188 (HA 188), some preliminary results were established[5] for the Ni-base alloy Haynes® Alloy 230 (HA 230). Also, during the course of this research, another study[7] indicated that the International Nickel Company Ni-base alloy Inconel 617 (IN 617) might likewise be suitable; hence, compatibility experiments involving this alloy were also initiated.

Because the potential corrosion problems associated with the space-based solar dynamic system are nontraditional, the three superalloys of concern were also annealed in static air at 1093 K for long periods of time. Comparisons of the behavior after air exposure with the results from the salt or vacuum exposures would then permit assessment of any extraordinary effects due to salt corrosion or evaporation of the volatile elements. This article presents the results of 4900, 10^4, and 22,500 h anneals in air at 1093 K on the structure of HA 188, HA 230, and IN 617. During the program, it was found that the geometry of the experiments resulted in innocuous surface attack for the majority of specimens given vacuum heat treatments. Hence, data for the vacuum-exposed alloys are also presented to characterize the influence of simple prolonged heating on the structure. A second article (accepted by the *Journal of Materials Engineering and Performance*) describes the effect of the air and vacuum 1093 K exposure on the 77 to 1200 K tensile properties of the three superalloys.

2. Experimental Procedures

Sheets of HA 188, HA 230, and IN 617 (Table 1) that were approximately 1.27 mm thick by 0.6 m by 1.2 m were purchased for this study. For simplicity and ease of fabrication, pin and clevis tensile-type specimens (108 mm long by 19 mm wide with a 31.8 mm by 9.8 mm gage section) were directly punched from the alloy sheet with the gage length parallel to the sheet rolling direction for HA 188 and HA 230. Due to a misinterpretation of the sheet orientation, the IN 617 samples were punched with their gage lengths perpendicular to the sheet rolling direction. After cleaning by hot vapor degreasing in

J.D. Whittenberger, NASA Lewis Research Center, Cleveland, OH 44135.

Table 1 Characterization of starting materials

Material	Vendor	Heat/lot	Composition, wt%
HA 188	Cabot Corp.	188061773	0.005B-0.11C-21.69 Cr-1.95Fe-0.048 La-0.72Mn-23.03 Ni-0.013P-<0.002 S-0.38Si-14.02W-Co
HA 230	Cabot Corp.	1830557171	0.004B-0.3Al-0.10 C-22.00Cr-1.22 Fe-0.009La-0.61Mn-1.29Mo-0.01P-<0.002 S-0.39Si-14.01W-Ni
IN 617	INCO Alloys International, Inc.	XX0130UK	1.05Al-0.002B-0.06 C-13.46Co-21.83 Cr-0.08Cu-1.66 Fe-0.14Mn-9.25 Mo-<0.001S-0.11 Si-0.24Ti-Ni
HS-25[15]	...	...	0.066C-20.00 Cr-1.65Fe-1.38 Mn-10.97Ni-0.30 Si-16.45W-Co

Table 2 Summary of exposures at 1093 K

	Exposure time, h	
	Vacuum	Air
HA 188	400, 2500, 4900, 10,000, and 22,500	4900, 10,000, and 22,500
HA 230	400, 2500, and 10,000	4900, 10,000, and 22,500
IN 617	400, 2500, and 7914	4900, 10,000, and 22,500

trichloroethane followed by immersion within an ultrasonic trichloroethane bath, all tensile specimens were individually weighed and measured. Samples were then placed into specimen racks constructed of the same alloy and recleaned. Figure 1 illustrates a typical rack containing more than 50 tensile-type specimens prior to exposure to either air or vacuum. Each sample weighed about 16 g and had approximately 33 cm^2 of surface area. Slots were cut into the specimen racks to maintain approximately 3 mm separation between individual samples.

The racks of specimens to be exposed in vacuum were placed on top of $LiF\text{-}CaF_2$ eutectic salt-filled corrosion capsules and introduced into a furnace.[5,6] Heat treatments were undertaken at 1093 K in a cryogenically pumped vacuum of $\sim 1.3 \times 10^{-4}$ Pa or better. None of these exposures were continuous; all experienced shutdowns due to loss of electrical power or cooling water, vacuum leaks, regeneration of the cryopumps, etc. In a like manner, the racks of alloy specimens heat treated in air at 1093 K were not continuously exposed; however, the number of disruptions were fewer than those experienced by samples within the vacuum furnaces. Following either air or vacuum exposure, the specimens were carefully removed from the racks with gloved hands and weighed. A summary of all the air/vacuum exposure conditions for each alloy is presented in Table 2. Although air exposure of all three alloys was conducted to 22,500 h, only HA 188 was given the longest heat treatment in vacuum. Only shorter vacuum heat treatments

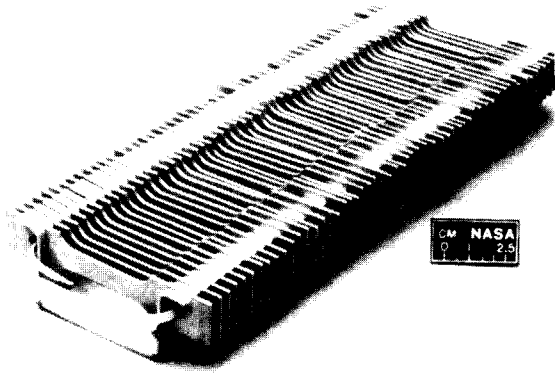

Fig. 1 Typical rack of superalloy tensile-test specimens prior to exposure.

of HA 230 and IN 617 were undertaken due to a redirection of the overall Space Station program.

Standard metallographic procedures and X-ray methods were used to characterize the starting, exposed, and tensile-tested materials. Polished metallographic sections of as-received HA 188 were immersion etched with a mixture of 80 ml HCl and 8 ml H_2O_2, whereas exposed material was electrolytically etched at 4 V and 0.5 A in 95 ml H_2O plus 5 ml HCl. All forms of HA 230 were electrolytically etched at 4 V and 0.5 to 0.75 A in a slightly diluted acid solution consisting of 33 ml HNO_3, 33 ml acetic acid, 33 ml H_2O, and 1 ml HF. IN 617 was also electrolytically etched at 4 V, 0.5 A for 2 to 3 s in a mixture consisting of 95 ml H_2O + 5 ml HCl.

3. Results

3.1 *As-Received Condition*

Ni-base alloy HA 230 and Co-base alloy HA 188 sheet were supplied in a solution treated condition, whereas Ni-base IN 617 was purchased in the cold rolled and annealed condition. Both HA 188 and IN 617 sheet possessed a normal silver metallic sheen, but the HA 230 had a dull oxide-like gray color due to the black anneal + pickling surface finish processing. Examination of this alloy by both metallography and X-ray diffraction techniques confirmed that the surface appearance was not due to a thick oxide layer. Polished and etched metallurgical sections revealed that the Haynes alloys[5] had reasonably uniform, equiaxed grain structures, where the average diameters were about 35 μm for HA 230 and 20 μm for HA 188. HA 188 possessed a consistent structure comprised of grains with numerous twins and a few second-phase particles; additionally, the sheet surface was smooth and essentially flaw free. HA 230, on the other hand, did not have a flat sheet surface; rather, this alloy contained pits as deep as 10 μm from the pickling process. Within the sheet interior, HA 230 had a relatively uniform, but sparse, dispersion of second-phase particles. IN 617, like HA 188, had a relatively flaw-free, smooth surface; however, ex-

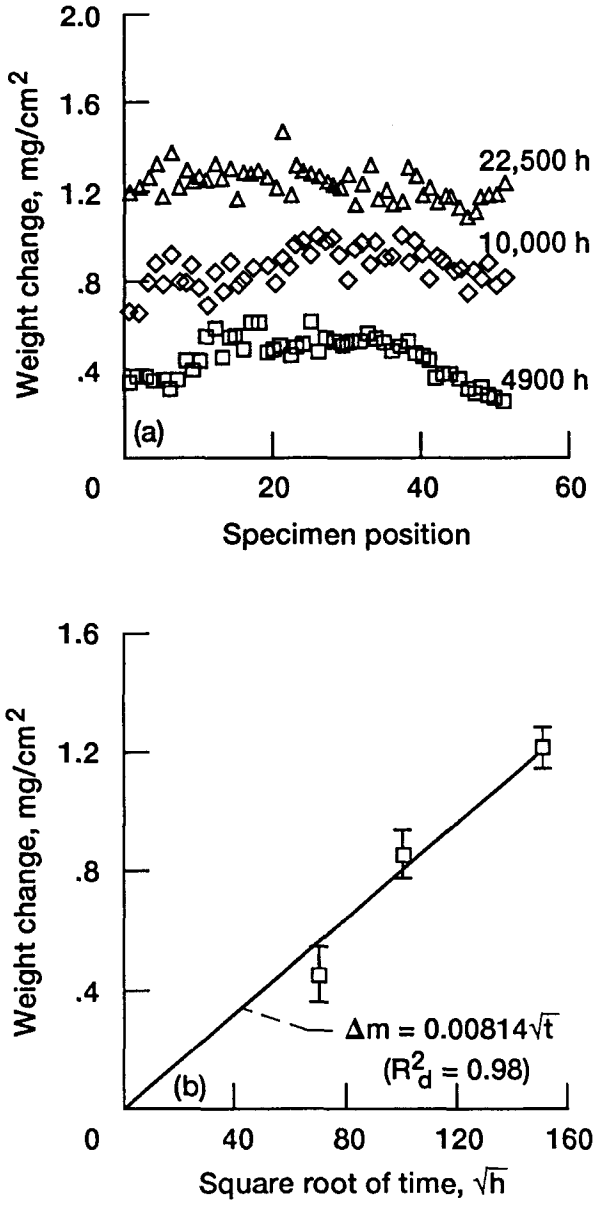

Fig. 2 Effect of long-term 1093 K air exposure on HA 188. (a) Specific weight change as a function of sample position and time. (b) Average specific weight change as a function of square root of time. Error bars in (b) represent ±one standard deviation.

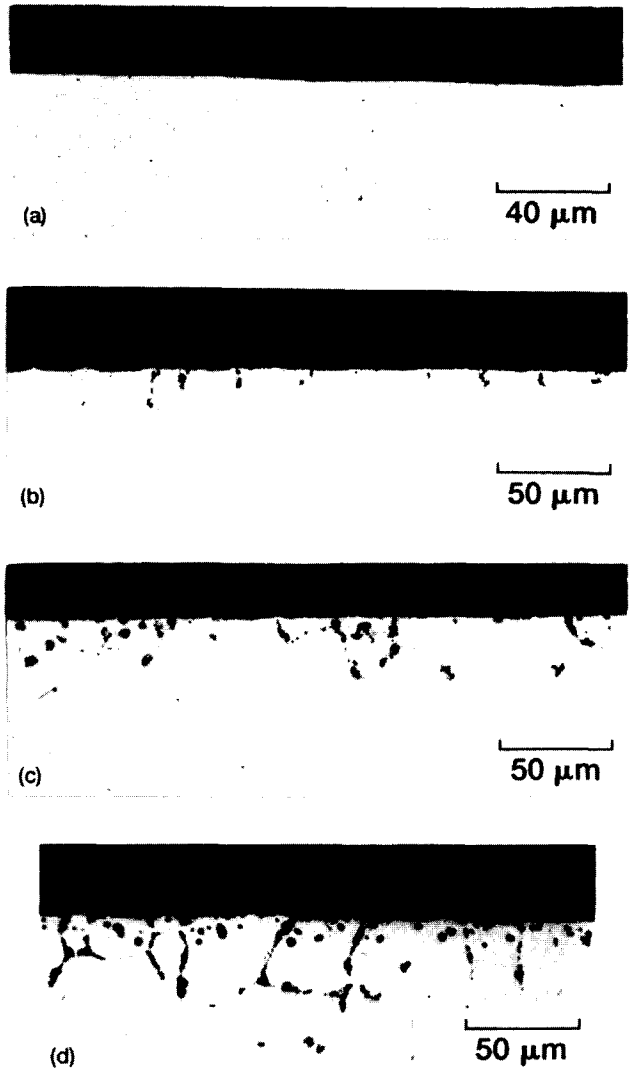

Fig. 3 Effect of long-term 1093 K air exposure on near-surface microstructure of HA 188. (a) As received. (b) 4900 h. (c) 10,000 h. (d) 22,500 h. All specimens are unetched.

amination of the microstructure revealed a thin layer of ~10 μm grains at the sheet surfaces and a much larger grain diameter (~85 μm) within the sheet interior. Unlike the Haynes alloys, as-received IN 617 had little evidence of any second phases.

3.2 *Effect of Heat Treatments on Exposed Surfaces*

After 1093 K air exposure, the surfaces of the three superalloys were covered with a dark, blackish scale that was comprised of Cr_2O_3 and Ni-base spinel for HA 230 and IN 617, or Co-base spinel for HA 188. The original bright shiny surfaces of HA 188 and IN 617 had a silvery matte metallic finish after 1093 K vacuum exposure, whereas HA 230 retained its original dull gray appearance after vacuum heat treatment.

3.2.1 HA 188

The specific weight change (as exposed – as received) for HA 188 heat treated in air at 1093 K is given in Fig. 2 as a function of time at temperature. As expected during isothermal oxidation under essentially static conditions, all specimens gained weight, which increased with exposure time. The data for individual samples in Fig. 2(a) indicate that position might have influenced the results for the 4900-h exposure, where specimens in the center of the rack have gained more weight than those located at the ends. Similar behavior, however, was not found after 10,000 or 22,500 h of air exposure. Ignoring any possible influence due to sample position, the average specific weight change for 1093 K air exposed HA 188 is shown as a function

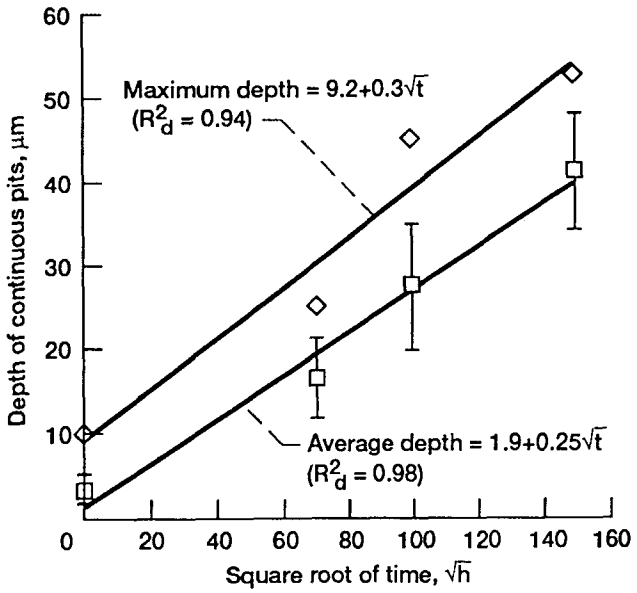

Fig. 8 Effect of long-term 1093 K air exposure on depth of intergranular porosity in HA 230. Error bars represent ±one standard deviation.

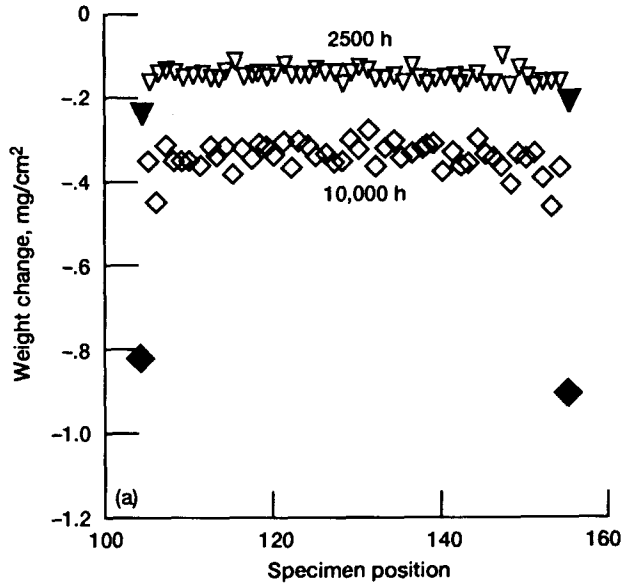

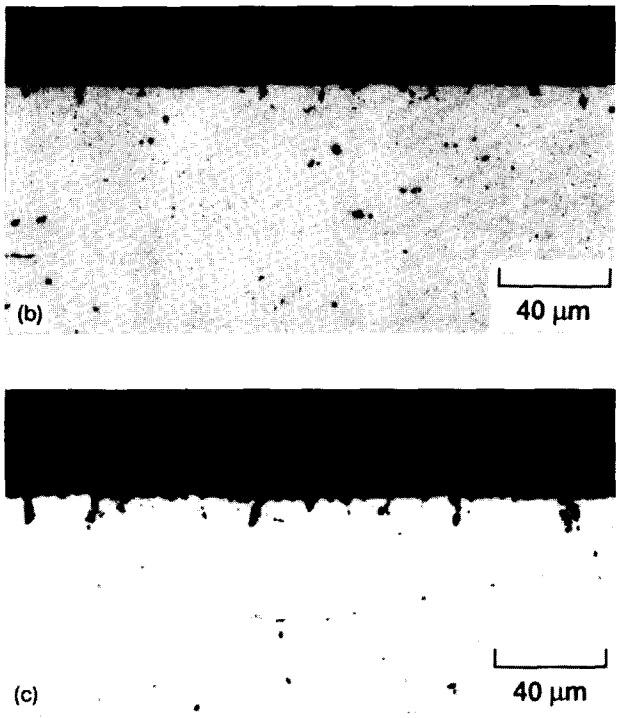

Fig. 9 Effect of long-term 1093 K vacuum exposure on HA 230. Specific weight change as a function of sample position and time (a), near-surface unetched microstructure in the as-received condition (b), and after 10,000 h (c).

sheet are shown in Fig. 7(a). During subsequent air exposure, the intergranular pits increase in depth and start to outline individual grains (Fig. 7b to d), whereas oxide films cover the surface. Isolated pores within the grains nearest the sheet surface can be seen after 4900 h (Fig. 7b) and 10,000 h (Fig. 7c) of exposure; however, they were less evident after 22,500 h (Fig. 7d). The depths of the pitting were measured, and the results are shown in Fig. 8, where both the maximum and average depths increased with the length of exposure. Using Eq 2, with the average and maximum pit depths being 3.5 and 10 μm, respectively, in the as-received HA 230 sheet, regression techniques indicate that the degree of attack increases with the square root of time. With the exception of the effects traceable to the pits in as-received HA 230, its near-surface structure after 1093 K heat treatment in air is similar to that found in HA 188 (Fig. 3 and 4).

The influence of 1093 K vacuum exposure on the weight change and the near-surface structure of HA 230 is presented in Fig. 9 after 2500 and 10,000 h. As was the case for HA 188 (Fig. 5a), the HA 230 end samples (denoted by filled symbols) lost much more weight than the specimens with neighbors on either side (Fig. 9a). Although the shielded specimens were subjected to basically innocuous heat treatments that resulted in minimal weight loss, some surface attack occurred. The narrow intergranular pits in the as-received alloy (Fig. 9b) are wider, and perhaps, deeper after 10,000 h (Fig. 9c). Additional prolonged 1093 K exposure to vacuum tends to roughen the overall HA 230 surface in a manner similar to that noted on HA 188 (Fig. 5c).

3.2.3 IN 617

The specific weight change for 1093 K air annealed IN 617 samples is presented in Fig. 10. Although HA 188 (Fig. 2) and HA 230 (Fig. 6) demonstrated substantial differences in weight gain among the periods of exposure, the weight changes for IN 617 after 4900 or 10,000 h are quite similar based on either individual (Fig. 10a) or averaged (Fig. 10b) results. Comparison of the data for IN 617 also indicates that the longest annealing period yields significantly more scatter than the shorter times at temperature; in fact, the 22,500 h air-exposed IN 617 exhibits the largest range of data found among the three superalloys.

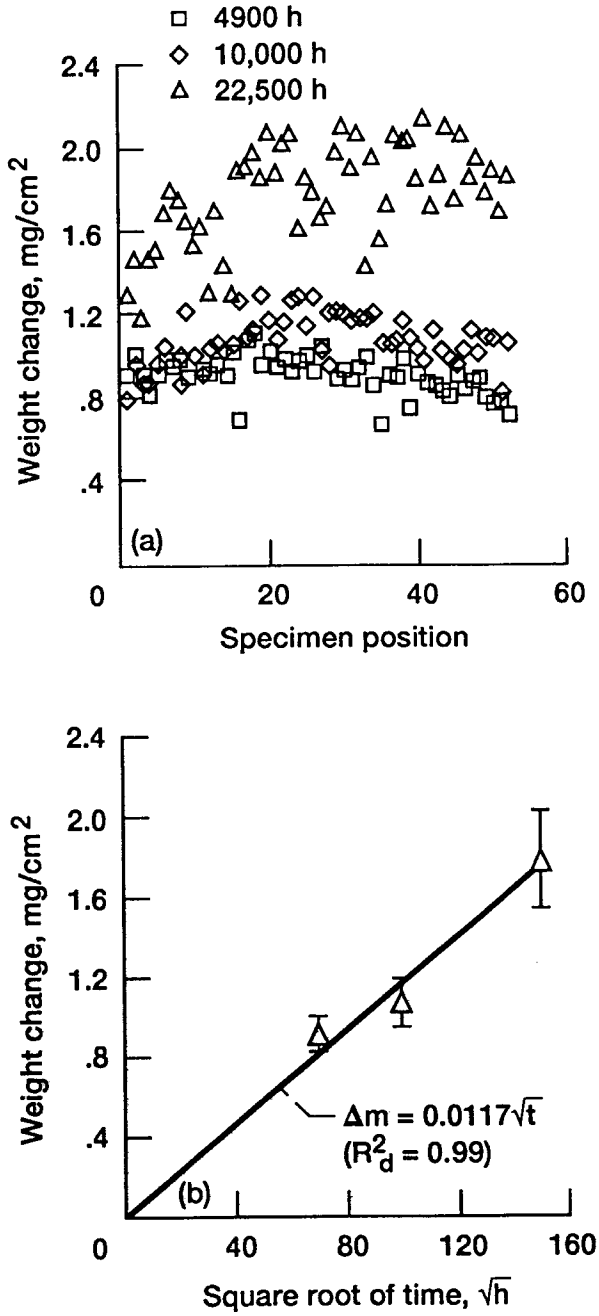

Fig. 10 Effect of long-term 1093 K air exposure on IN 617. (a) Specific weight change as a function of sample position and time. (b) Average specific weight change as a function of square root of time. Error bars in (b) represent ±one standard deviation.

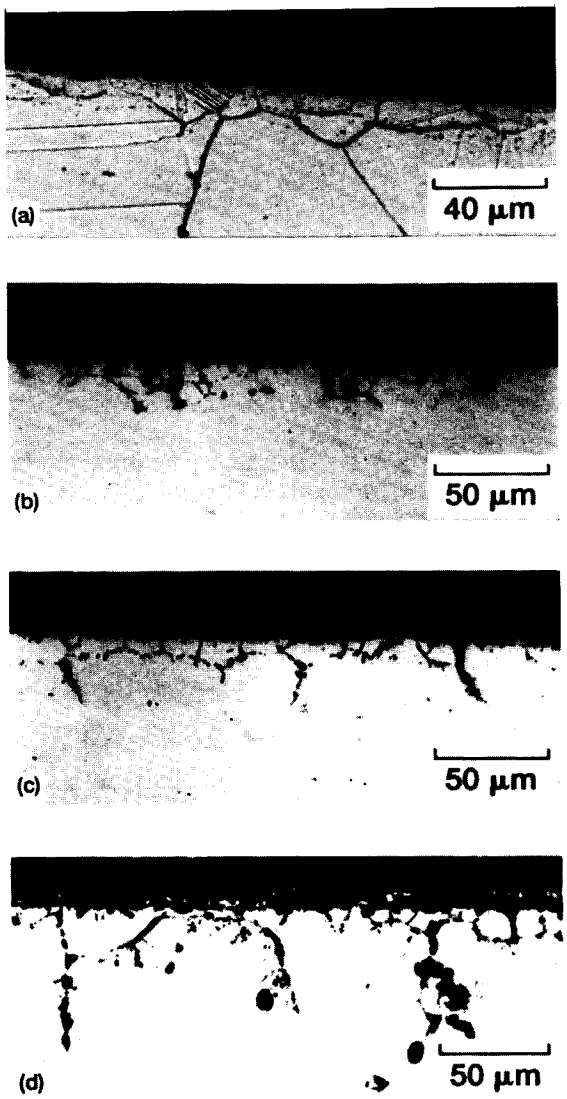

Fig. 11 Effect of long-term 1093 K air exposure on near-surface microstructure of IN 617. (a) As received. (b) 4900 h. (c) 10,000 h. (d) 22,500 h. All specimens except (a) are unetched.

Despite the similarity in the 4900 and 10,000 h results and the deviations in the 22,500 h data, the averaged specific weight changes (Fig. 10b) can be described by Eq 1. Examination of the microstructure of IN 617 heat treated in air indicated that the small grain structure at the sheet surfaces (Fig. 11a) provided sites for subsequent intergranular attack (Fig. 11b). The underlying large grain microstructure, however, tended to restrict the extent of the intergranular attack (Fig. 11 c and d). In addition to showing that deep intergranular penetrations can occur in IN 617 after 22,500 h of air exposure, Fig. 11(d) also reveals that the cracks are oxide filled. Presumably, the intergranular attack paths after 4900 h (Fig. 11b) and 10,000 h (Fig. 11c) were also filled with oxides, which pull-out during polishing.

Because the thin layer of small grains over larger grains affected the nature of the intergranular attack of IN 617, calculations of the "average" length of intergranular oxidation for the 10,000 h (Fig. 11c) and 22,500 h (Fig. 11d) air-exposed alloy were restricted to those cracks that clearly extended beyond the thin surface grain region. Even with this restriction, neither the average length nor maximum length of intergranular attack in IN 617 exhibited a conclusive dependency on the square root of time of exposure (Fig. 12), as reflected by the relatively low co-

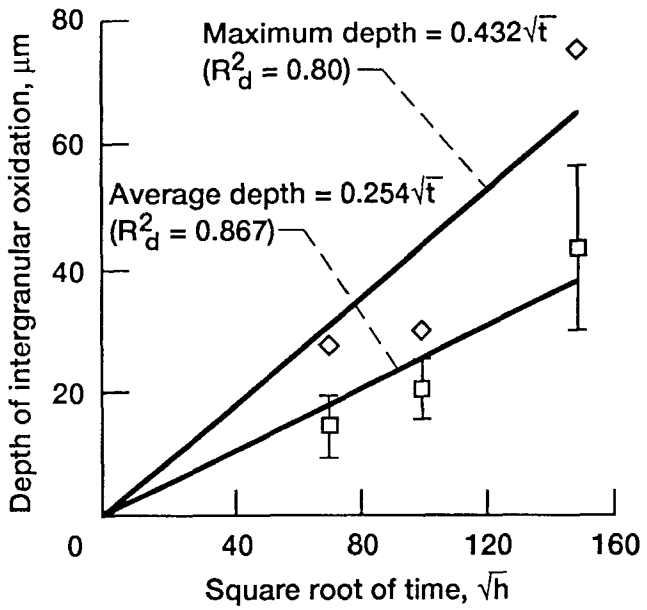

Fig. 12 Effect of long-term 1093 K air exposure on depth of intergranular porosity in IN 617. Error bars represent ±one standard deviation.

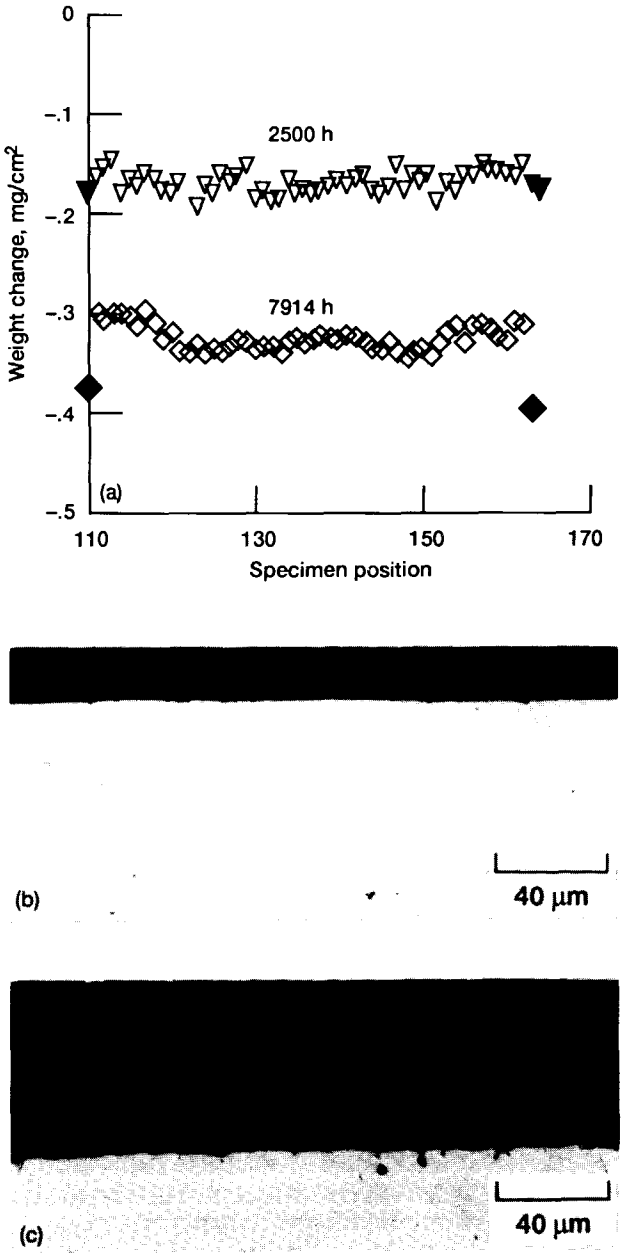

Fig. 13 Effect of long-term 1093 K vacuum exposure on IN 617. Specific weight change as a function of sample position and time (a), near-surface unetched microstructure in the as-received condition (b), and after 8914 h (c).

efficients of determination for the fits. Such behavior is contrary to that for either HA 188 (Fig. 4) or HA 230 (Fig. 8).

A further difference in the performance of IN 617 in comparison to either HA 188 or HA 230 can be seen in the specific weight change data for 1093 K vacuum-exposed IN 617 in Fig. 13(a). Although the weight loss for IN 617 did increase with exposure time, the end samples did not lose significantly more mass than the shielded samples. In particular, the IN 617 end samples after 7914 h of vacuum heat treatment lost ~20% more weight than a typical shielded specimen. This behavior contrasts with that for the other two long-term vacuum-exposed superalloys (Fig. 5a and 9a), where the end samples lost approximately twice the weight of the specimens with neighbors on either side. Examination of the near-surface microstructure for a shielded specimen demonstrated little change between the as-received condition (Fig. 13b) and that after 7914 h of vacuum annealing (Fig. 13c), except for a slight roughening and an occasional shallow pit or isolated pore.

3.3 *Effect of Heat Treatment on Internal Microstructure*

Typical etched as-received and 1093 K heat treated microstructures are presented in Fig. 14 to 16 for HA 188, HA 230, and IN 617, respectively. The heavily twinned structure of as-received HA 188, which contains only a few inter- and intragranular precipitates (Fig. 14a), undergoes heavy precipitation of M_6C and Laves phases[8] within the grains and on the grain boundaries after 1093 K heat treatments (Fig. 14b). The 1093 K exposure of HA 230 also results in significant precipitation (Fig. 15b) of metal carbides ($M_{23}C_6$)[8] compared to the relatively clean as-received material (Fig. 15a). In contrast, the amount of second phase formation ($M_{23}C_6$)[9] within IN 617 after exposure (Fig. 16c and d) is substantially less than that found in either HA 188 (Fig. 14b) or HA 230 (Fig. 15b). Furthermore, comparison of the IN 617 as-received microstructure (Fig. 16a and b) with that after long-term 1093 K annealing (Fig. 16 c and d) confirms the relative phase stability of this alloy.

Average grain size diameters have been determined by the circle intercept method for each alloy as a function of exposure time and environment. These data are presented in Fig. 17 where, for convenience, the square root of time is used as the abscissa. As would be intuitively expected, environment did

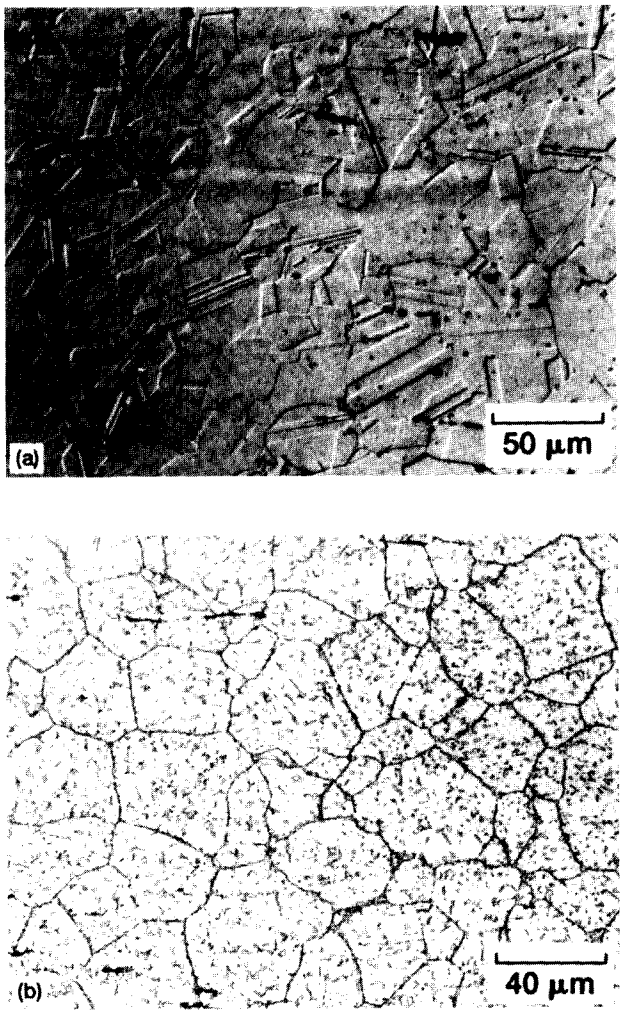

Fig. 14 Effect of long-term 1093 K exposure on the internal microstructure of HA 188. (a) As received. (b) 22,500 h. Both specimens are etched. (a) Taken under differential interference conditions, (b) taken under bright-field conditions.

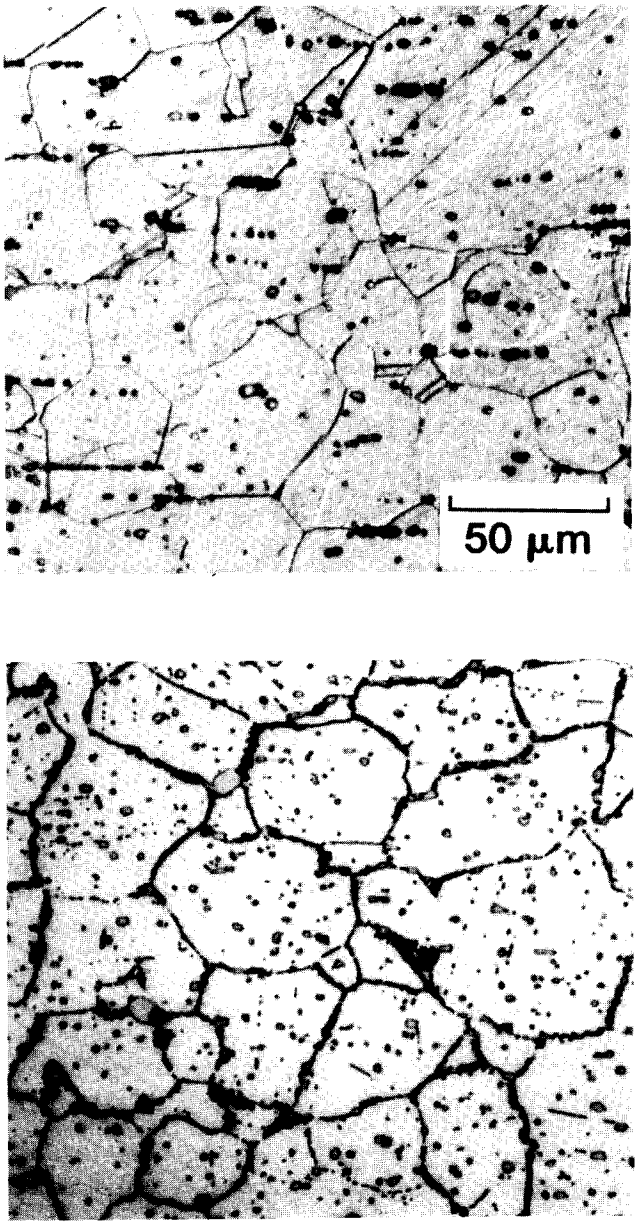

Fig. 15 Effect of long-term 1093 K exposure on the internal microstructure of HA 230. (a) As received and (b) 22,500 h. Both specimens are etched. (a) Taken under differential interference conditions; (b) taken under bright-field conditions.

not influence the size of the grain structure for any of the three superalloys (Fig. 17). In the case of HA 188 (Fig. 17a), exposure time might have affected the average grain size, where it increased about 50% from 20 to ~30 μm during 1093 K annealing. On the other hand, the grain dimensions for HA 230 (Fig. 17b) and IN 617 (Fig. 17c) did not change even after 22,500 h at temperature.

4. Discussion

In general terms, the structure of the three superalloys was not affected in any unexpected manner by long-term exposure at 1093 K. Heat treatment in air produced oxide scales and surface-connected intergranular pits or oxides, whereas essentially only surface roughening took place in shielded, vacuum annealed samples. Both HA 188 (Fig. 14) and HA 230 (Fig. 15) exhibited significant second-phase precipitation, which was expected.[5,6] IN 617 precipitated less second phases (Fig. 16) than either HA 188 or HA 230. Furthermore, the amount of carbide observed in the current heat of IN 617 under zero stress for 10,000 h was much less than that formed under low stress 10,000 h conditions between 1033 and 1144 K.[9] Because the only significant difference in composition between the two heats was the titanium level, which was 0.24 wt.% in this study and 0.41 wt% in Ref 9, there should be more primary carbide and less $M_{23}C_6$ in the material used in the study by Mankins et al.[9] Therefore, it is probable that the abundance of second

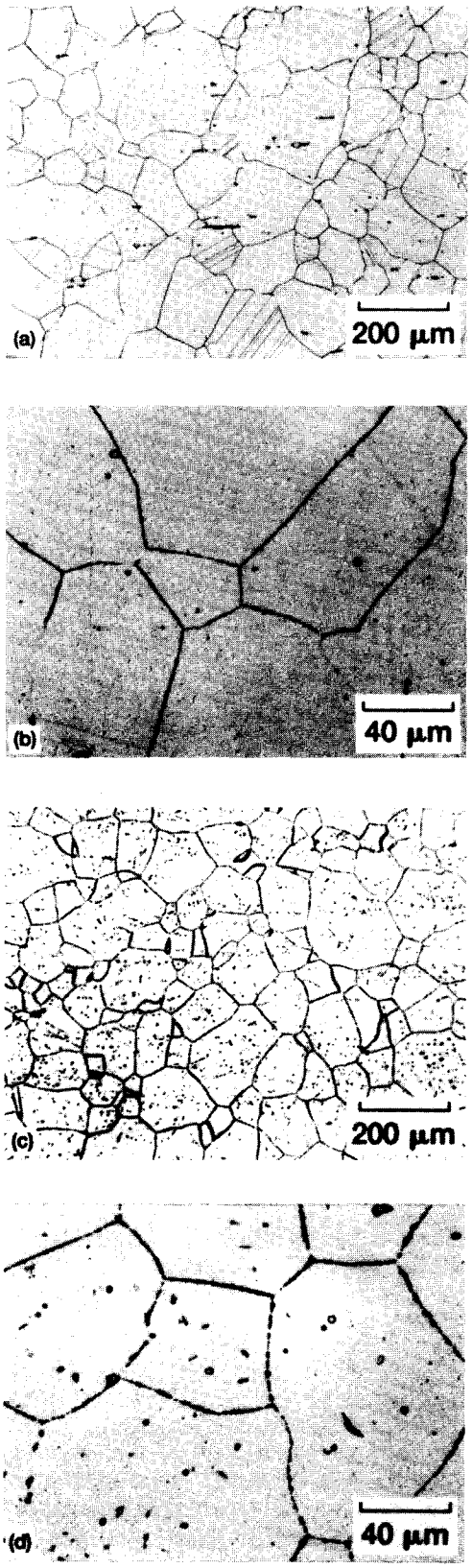

Fig. 16 Effect of long-term 1093 K exposure on the internal microstructure of IN 617. (a) and (b) As received. (c) and (d) 10,000 h. All specimens are etched and taken under bright-field conditions.

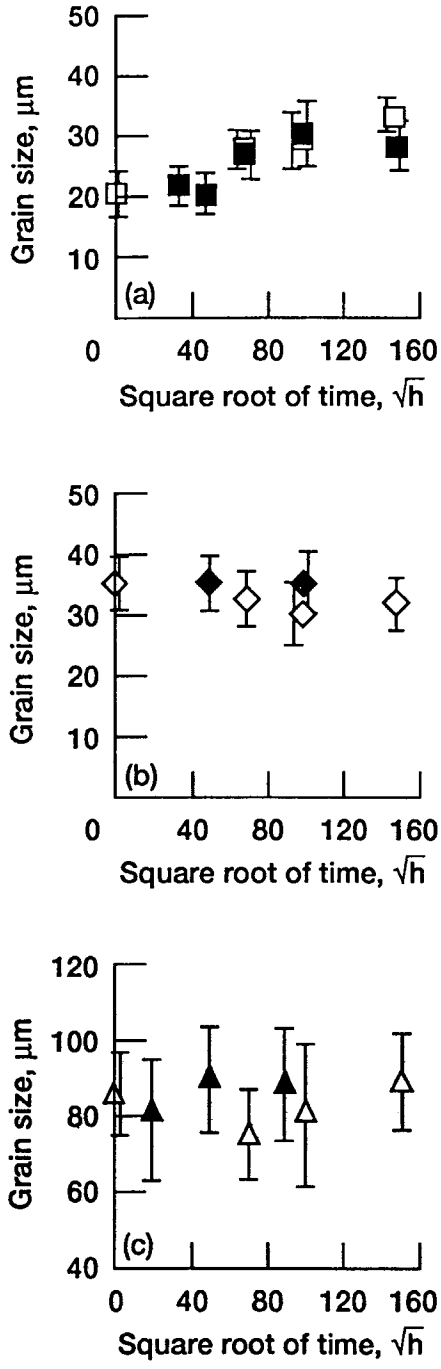

Fig. 17 Effect of long-term 1093 K exposure on the average grain size of (a) HA 188, (b) HA 230, (c) IN 617. Open symbols denote air exposure, whereas filled symbols denote vacuum exposure. Error bars represent ±one standard deviation.

phases in Ref 9 is the result of precipitation on dislocations rather than chemistry.

4.1 *Air Exposure*

Long-term 1093 K air exposure of HA 188 and HA 230 results in oxide scales, some intergranular porosity, and surface-

Table 3 Parabolic scaling constants for HA 188 and IN 617

Alloy	Temperature, K	k_p, mg/cm^2/h	Conditions	Ref
HA 188	1093	6.6×10^{-5}	...	This study
	1088	5.3×10^{-4}	Ten 1000-h cycles	10
	1093	1.1×10^{-4}	700 cycles at 5 h each	11
IN 617	1093	1.4×10^{-4}	...	This study
	1088	2.8×10^{-4}	Ten 1000-h cycles	10

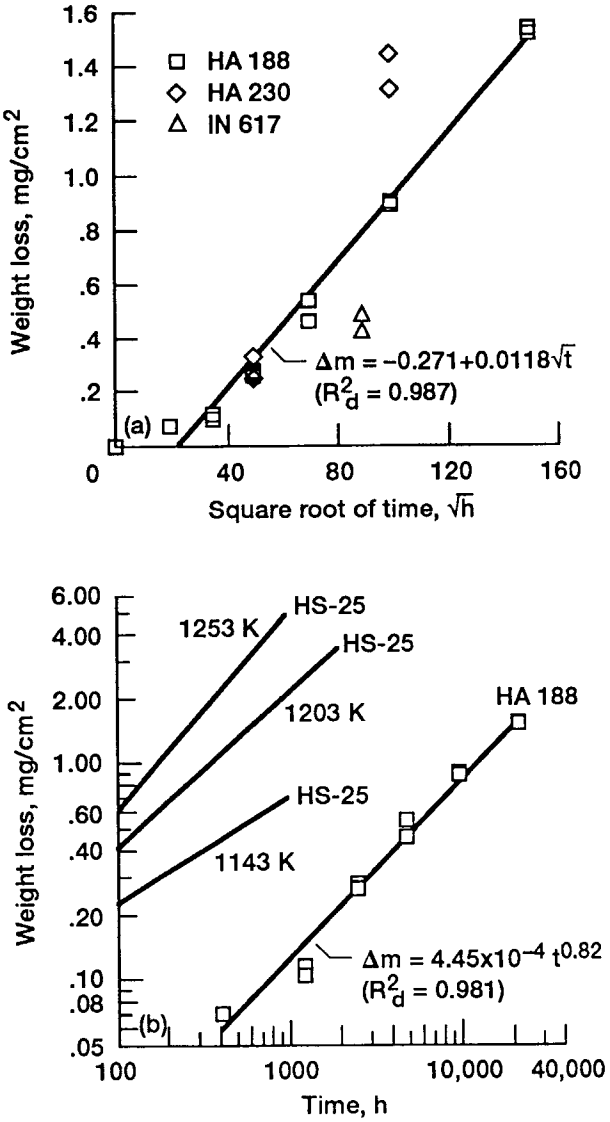

Fig. 18 Estimated specific weight loss in vacuum as a function of time (a) for the three superalloys at 1093 K and (b) comparison of the behavior of HS-25 between 1253 and 1143 K to that of HA 188 at 1093 K.

connected intergranular pits. The long-term exposure of IN 617 yielded similar effects, except that there is clear evidence that the intergranular attack is the result of oxidation (Fig. 11d). Although re-examination of the air-exposed HA 188 and HA 230 samples still indicates that the intergranular attack is in the form of connected porosity, it is possible that the cracks were filled with oxides that subsequently pulled out during polishing. Whether oxide filled or a collection of pores, the surface-connected pits are probably the most serious oxidation-related defect, with the maximum lengths approaching 50 to 70 μm for the alloys after 22,500 h at temperature (Fig. 4, 8, and 12). For the current ~1.3 mm thick sheet, this depth represents, at most, a 10% loss in load-bearing area; therefore, these defects probably would not seriously affect the performance of the material. However, if 0.25 mm sheet stock were under consideration for use, a 22,500-h exposure to air at 1093 K could mean that, in some areas, only 60 to 40% of the original cross section would support structural loading. Such reductions could be catastrophic.

X-ray examination of the oxides formed on each superalloy indicated that the scales consisted of chromia and spinels, which is in agreement with previous studies[10-12] undertaken at or near 1093 K in air. Comparison of the weight gain results reveals that HA 188 (Fig. 2) has slightly more oxidation resistance than HA 230 (Fig. 6), which is in turn somewhat better than IN 617 (Fig. 10). Ganesan and Smith[12] also found HA 188 to have a small advantage in oxidation resistance over IN 617 under cyclic conditions in an air + 5% water vapor environment at 1173 K. Barrett,[10] on the other hand, reported that IN 617 was slightly better than HA 188 after ten 1000-h cycles in air at 1088 K. The current ranking of HA 188 > HA 230 > IN 617 is reflected in the values of the square roots of the parabolic scaling constants, $\sqrt{k_p}$, presented in Fig. 2, 6, and 10, respectively. Furthermore, as shown in Table 3, the parabolic scaling constants determined for HA 188 and IN 617 in this study agree well with those determined by Barrett et al. under near-isothermal conditions at 1088 K[10] and cyclic conditions at 1093 K.[11]

Clearly, the kinetics of weight gain during 1093 K air exposure are dependent on the square of time for all three superalloys (Fig. 2b, 6b, and 10b). Furthermore, with the possible exception of IN 617, the rates of growth for the average and longest intergranular surface-connected pits/oxides are also a function of the square root of time (Fig. 4, 8, and 12). Thus, oxidation of HA 188, HA 230, and IN 617 appears to be diffusion controlled, and the current results can be justifiably extrapolated to much longer exposure times.

4.2 *Vacuum Exposure*

With the exception of the samples at the ends of the racks (Fig. 1), none of the vacuum annealed specimens underwent true vacuum exposure. Because the majority of tensile-type test samples had neighbors on both sides in very close proximity, volatilized elements were simply passed back and forth; the net result being very little mass lost even after 22,500 h in vacuum

Table 4 Summary of weight change and microstructural results for three superalloys exposed to air or vacuum at 1093 K

Alloy	Observation
Air and vacuum	
HA 188, HA 230	Significant grain boundary and intragranular carbide precipitation
IN 617	Minor carbide precipitation
HA 188	Grain growth (20 to 30 μm in 22,500 h)
HA 230, IN 617	No grain growth
Air	
HA 188, HA 230, IN 617	Weight gain increased with $\sqrt{t}$; depth of surface-connected grain boundary pitting/oxidation increased with $\sqrt{t}$
Vacuum	
All (shielded)	Weight loss increased with time
HA 188 (unshielded)	Weight loss increased with $\sqrt{t}$
IN 617	Weight loss for shielded and unshielded samples similar

at 1093 K (Fig. 5a). Hence, the 1093 K vacuum exposures in this study for most HA 188, HA 230, and IN 617 specimens were basically heat treatments in a very innocuous atmosphere.

The specimens at the ends of the racks (Fig. 1) have surfaces that are not shielded, and these faces can lose all volatilized matter. Estimates for the specific mass loss for the three superalloys during 1093 K vacuum exposures can be made from sample weight loss data and the assumption that the weight loss experienced by the shielded side of each end sample (i.e., half the total area) is given by half the arithmetic average of the weight loss data for all the shielded specimens. The results for these calculations are presented in Fig. 18(a) as a function of the square root of time. Because only the two IN 617 end samples from 7914 h vacuum exposure (Fig. 13(a) demonstrated a larger loss than an average specimen, only one set of data are shown for this alloy. The limited vacuum annealing of HA 230 (Fig. 9a) also restricted information on this alloy; hence, only results from 2500 to 10,000 h are presented in Fig. 18(a). The largest range of vacuum exposures was obtained for HA 188 (Fig. 5a and Ref 5), and estimates for the evaporative losses are available from 400 to 22,500 h at 1093 K. Based on the data in Fig. 18(a), it appears that IN 617 is subject to less volatilization than HA 188, while more mass is lost from HA 230 than from HA 188. This ranking can be explained on the basis of the alloy chemistry (Table 1), assuming that Mn and Cr are the volatilized elements. On an atomic percent basis (and even weight percent), the summations of Cr and Mn compositions reveal that alloys rank as IN 617 < HA 188 < HA 230; therefore, the resistance to evaporation should also follow this order.

Due to the restricted results for HA 230 and IN 617, no effort was made to determine their behavior as a function of time. Results of the fit of HA 188 as a diffusion-controlled process (i.e., the form of Eq 1) were not very successful both in a visual sense and in terms of the coefficient of determination (0.92). However, if the data between 400 and 22,500 h are fitted to a modified diffusion-controlled process, where

$$\Delta m = C + D\sqrt{t} \quad [3]$$

with C and D being constants, a high coefficient of determination and a good visual fit (Fig. 18a) are produced. In this case, the constant C and the first 400 h of exposure can be viewed as the consequence of surface films on the as-received HA 188 sheet. Previous studies of iron-, cobalt-, and nickel-base alloys[4,13,14] have shown that oxide films can prevent evaporation of volatile elements during vacuum annealing. Such protection is, nonetheless, only temporary, and the normal volatilization behavior eventually takes place. Therefore, the first few hundred hours of 1093 K vacuum exposure can be rationalized as the time required to break down the surface film on the as-received HA 188, which inhibited evaporation.

Bourgette[15] has studied volatilization from the cobalt-base alloys Haynes Alloy 25 (HS-25, Table 1) as a function of temperature in a vacuum on the order of 10^{-6} Pa. His lower temperature specific weight loss results for HS-25 are presented in Fig. 18(b) along with the present 1093 K HA 188 values. Following Bourgette,[15] the data are shown in a log-log form of

$$\Delta m = Et^p \quad [4]$$

where E and p are constants, and as indicated in Fig. 18(b), Eq 4 can also describe the HA 188 results well. The behavior of HA 188 at 1093 K follows the general trend established by the HS-25 vacuum exposed at higher temperatures, where the degree of volatilization decreases with decreasing temperature. Visual comparison of the slopes of the various curves, however, suggests that evaporation is more rapid from HA 188 at 1093 K than it would be from HS-25 at this temperature. As was the case for ranking the volatility of the three superalloys examined in this study, this apparent difference could also be due to the volatile element content where the summation of Cr and Mn compositions is less for HS-25 than HA 188 (Table 1).

5. Summary

Long-term 1093 K exposure changed the microstructure and surface structure of unstressed HA 188, HA 230, and IN 617. These modifications are outlined in Table 4 as a function of alloy and environment. With either air or vacuum exposure, significant precipitation of second-phase carbides occurred in the Co-base alloy HA 188 and the Ni-base alloy HA 230; however, much less precipitation was found in the exposed Ni-base alloy IN 617. Although some grain growth occurred in HA 188, no changes in the grain size of either HA 230 or IN 617 was observed after 22,500 h at temperature. Oxidation during air heat treatments led to weight gains from the formation of chromia + spinel scales and surface-connected grain boundary pits/oxides in all three superalloys. Both the weight gain and depth of intergranular attack were dependent on the square root of time, which is indicative of diffusion-controlled phenomena. The effect of vacuum exposure on the superalloys was dependent on the test geometry. If neighboring samples were in close proximity, weight losses due to evaporation occurred and increased with time of exposure; however, the overall effect was minor for all alloys. The back and forth transfer of volatile elements from one neighbor to another prevented unrestricted mass loss

and thus shielded the alloys. The samples at the ends of the specimen racks permitted the effects of an unfettered vacuum environment to be estimated. Based on the data for HA 188, the weight loss is diffusion controlled (proportional to the $\sqrt{t}$) once the inhibiting effects of surface films on the as-received alloys are broken down.

References

1. T.L. Labus, R.R. Secunde, and R.G. Lovely, Solar Dynamic Power Module Design, Paper No. 899277, *IECEC '89*, Vol 1, IEEE, 1989, p 299-307
2. H.J. Strumpf, R.P. Rubley, and M.G. Coombs, Material Compatibility and Simulation Testing for the Brayton Engine Solar Receiver for the NASA Space Station Freedom Solar Dynamic Option, Paper No. 899076, *IECEC '89*, Vol 2, IEEE, 1989, p 895-903
3. R.C. Schulze, NASA CR-54781, 1965
4. D.T. Bourgette and H.E. McCoy, *Trans. ASM*, Vol 59, 1966, p 324-339
5. J.D. Whittenberger, *J. Mater. Eng.*, Vol 12, 1990, p 211-226
6. J.D. Whittenberger, *J. Mater. Eng. Perf.*, Vol 1, 1992, 469-482
7. J.D. Cotton and L.M. Sedgwick, Compatibility of Selected Superalloys with Molten LiF-CaF_2 Salt, Paper No. 899235, *IECEC '89*, Vol 2, IEEE, 1989, p 917-921
8. M. Rothman, Haynes International, personal communication
9. W.L. Mankins, J.C. Hosier, and T.H. Bassford, *Metall. Trans.*, Vol 5, 1974, p 2579-2590
10. C.A. Barrett, *Environmental Degradation of Engineering Materials*, Virginia Polytechnical University, 1977, p 319-327
11. J.R. Stephens and C.A. Barrett, NASA TM-83609, 1984
12. P. Ganesan and G.D. Smith, *J. Mater. Eng.*, Vol 9, 1988, p 337-343
13. D.T. Bourgette, ORNL-TM-13677, 1964
14. L.A. Charlot and R.E. Westerman, *Corrosion*, Vol 23, 1967, p 50-56
15. D.T. Bourgette, ORNL-TM-1786, 1967